

# Finite element analysis of damage in pipeline bends

A.E. Swart

Corresponding address: CORUS RD&T, PO Box 10000, 1970CA, IJmuiden, the Netherlands

S.A. Karamanos

University of Thessaly, Fac. of Mechanical & Industrial Engineering, Greece

A. Scarpas

Delft University of Technology, Fac. of Civil Engineering and Geosciences, the Netherlands

J. Blaauwendraad

Delft University of Technology, Fac. of Civil Engineering and Geosciences, the Netherlands

**The present paper describes a numerical formulation for the analysis of damage in steel pipeline bends. In particular, the numerical implementation of Gurson plasticity model is described in the framework of a special element, referred to as “tube element”. This is a three-node element, which simulates pipe behavior combining longitudinal deformation with cross-sectional ovalization and warping. The numerical results obtained with the tube elements are compared with results obtained with selective integrated Heterosis elements. The constitutive equations are integrated through an Euler-backward numerical scheme, enforcing the condition of zero stress in the radial direction of the pipe. Results for isotropic hardening have been obtained.**

*Key words: Tube element, Gurson model, computational plasticity, damage*

## 1 Introduction

Gasses and fluids are transported via an extensive infrastructure of steel pipelines. In the design of pipeline systems the use of elbows (pipe bends) is important to cross obstacles, like the many rivers and canals in the Netherlands, as shown in Figure 1. As shown by the pioneering work of Von Karman, the flexural rigidity of pipe bends is smaller than that of a straight pipe. This added flexibility makes them able to sustain significant deformations

and therefore suitable to accommodate thermal expansions and absorb other externally induced loads in the pipeline.

The pipelines can be subjected to combinations of soil pressures, temperature variations and soil settlements, which cause permanent plastic bending moments. These bending moments cause the circular cross-section of the elbows to ovalize. In addition, the initially plane cross section of the bend tends to deform out of its own plane, which is also known as warping. In combination with alternating levels of internal pressure, the variation of the stresses in the longitudinal and the radial directions may lead to the initiation and progressive development of plasticity.



*Figure 1: Pipeline crossing a canal (photo: ir. A.M. Gresnigt)*

In structural steels, after the onset of plasticity, progressive material damage can initiate in the form of micro-void nucleation. The micro-voids in the metallic material can eventually grow and coalesce leading to cleavage cracking. The initiation and growth of voids within a metallic material can be elegantly simulated by means of the Gurson material model [3]. This plasticity based material model contains the classical von Mises model and is capable of reproducing accurately various aspects of metallic material post-yield response. According to this model, the real material consists of intact material, carrying the stresses, and voids. A numerical implementation of this model has been presented by Aravas [1].

Herein, the finite element implementation of the Gurson model is discussed in the framework of a special finite element, the “tube element”, which describes the tube deformation in a rigorous manner, combining beam-type deformation with cross-sectional deformation.

## 2 Finite element formulation

In principle, finite element shell models can be employed to obtain very accurate solutions for the nonlinear analysis of piping structures. To reduce the cost of analysis, various different formulations of “simple” pipe elbow elements have been developed. Von Karman [9] analyzed elbows subjected to a constant in-plane bending moment and showed that the cross-section deforms to an oval. In the analysis, the longitudinal and circumferential strains due to ovalization of the cross section are superimposed on curved beam theory displacements. Vigness [10] later showed that out-of-plane flexibility factors were identical to the in-plane values. Clark and Reissner [11] proposed equations for the bending of a toroidal shell segment and, derived from an asymptotic solution, introduced the flexibility and stress factors. Among others, Rodabough and George [12] extended the work by Von Karman and used the potential energy approach to investigate the effects of internal pressure for the case of in-plane bending under a closing moment. They formulated the pressure reduction effect on the flexibility and stress intensification factors. With zero pressure their results reduce to von Karman’s.

Bathe and Almeida [13, 14] proposed an efficient formulation for a tube bend element with axial, torsional, and bending displacements and the Von Karman ovalization deformations. The main characteristic of the tube element is the combination of longitudinal (beam-type) with cross-sectional deformation (ovalization). Based on this formulation, Karamanos and Tassoulas [8] developed a nonlinear three-node tube element, capable of describing accurately in-plane and out-of-plane deformation. This element has been used successfully for predicting the ultimate capacity of inelastic tubes under the combined action of thrust, moment and pressure. The isoparametric beam finite element concept is used to describe longitudinal deformation, with three nodes defined along the tube axis, as shown in Figure 2. Geometry and displacements are interpolated using quadratic polynomials.

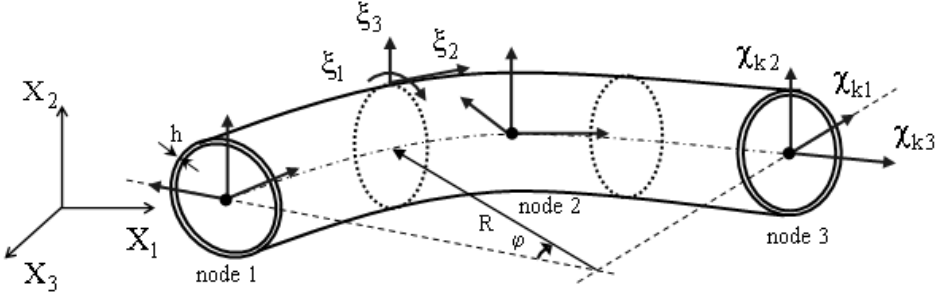


Figure 2: Coordinate systems tube finite element

The location of a point before deformation is determined by the position vector  $\mathbf{X}$ , defined in a Cartesian global axes system  $\{X_i, i = 1, 2, 3\}$ , as shown in Figure 2. The tube element is assumed to be symmetric with respect to the  $X_1 - X_3$  plane. Regarding a beam rotation about the  $X_2$  axis, each node possesses three degrees of freedom (two translational and one rotational), which define its position and orientation.

At each element node  $k$  a local Cartesian axes system  $\{X_{ki}; i = 1, 2, 3\}$  is defined. This system is used as a reference frame for the cross-sectional deformation parameters.

At each integration point a local system is introduced through the use of coordinates  $\xi_i$  in the hoop, longitudinal and along the thickness direction (denoted as  $\xi_1$ ,  $\xi_2$  and  $\xi_3$  respectively), as presented in Figure 2. Due to symmetry, only half of the tube is analyzed ( $-\pi/2 \leq \xi_1 \leq \pi/2$ ). The  $\xi_2$  axis spans between (0, +1), where the  $\xi_3$  axis spans between (-1, +1).

### 2.1 Initial element geometry

The pipe thickness  $h$  is assumed to be constant and a reference line is chosen within the cross-section. The initial location of any point within the element can therefore be interpolated on the basis of the node coordinates, the reference line and the thickness via:

$$\mathbf{X} = \sum_{k=1}^3 \mathbf{A}_k N_k(\xi_2) + \sum_{k=1}^3 \mathbf{r}_k(\xi_1) N_k(\xi_2) + \sum_{k=1}^3 \xi_3 \frac{h}{2} \mathbf{n}_k(\xi_1) N_k(\xi_2), \quad (1)$$

where  $N_k(\xi_2)$  represents the corresponding Lagrangian quadratic interpolation functions,  $\mathbf{A}_k$  the position vector of node  $k$  in the global axes system, and  $\mathbf{n}_k(\xi_1)$  the "in-plane"

outward normal of the reference line. The position vector of the undeformed reference line at the cross-section corresponding to node  $k$  can be expressed as:

$$\mathbf{r}_k(\xi_1) = x_{k,1}\chi_{k,1} + x_{k,2}\chi_{k,2} + x_{k,3}\chi_{k,3}, \quad (2)$$

where, in the original configuration,

$$\begin{aligned} x_{k,1}(\xi_1) &= r \cos \xi_1 \\ x_{k,2}(\xi_1) &= r \sin \xi_1 \\ x_{k,3}(\xi_1) &= 0, \end{aligned} \quad (3)$$

with  $r$  the radius of the undeformed reference line.

## 2.2 Updated element geometry

For the purposes of the present study, bending is applied about the axis  $X_2$  (i.e.  $X_1 - X_2$  is the plane of bending). The deformed tube axis is defined by:

$$\mathbf{x}_c(\xi_2) = \sum_{k=1}^3 \mathbf{x}_k N_k(\xi_2), \quad (4)$$

where  $\mathbf{x}_k$  is the position vector of node  $k$ . To describe cross-sectional deformation, pipe thickness is assumed to be constant and a reference line is chosen within the cross-section. Both in-plane (ovalization) and out-of-plane (warping) cross-sectional deformations are considered. For in-plane deformation of the tube element, fibers initially normal to the reference line are assumed to remain normal to the reference line.

Following the formulation by Brush and Almroth [2], the position vector of the reference line at the current configuration can be expressed in terms of the radial and tangential displacements. The updated components of  $\mathbf{r}_k(\xi_1)$  at the deformed cross-section, as depicted in Figure 3, are

$$\begin{aligned} x_{k,1}(\xi_1) &= [r + w(\xi_1)] \cos \xi_1 - v(\xi_1) \sin \xi_1 \\ x_{k,2}(\xi_1) &= [r + w(\xi_1)] \sin \xi_1 + v(\xi_1) \cos \xi_1 \\ x_{k,3}(\xi_1) &= \psi(\xi_1). \end{aligned} \quad (5)$$

In the above expressions  $w(\xi_1)$ ,  $v(\xi_1)$  and  $\psi(\xi_1)$  are displacements of the reference line in the radial, tangential and out-of-plane (axial) direction, respectively.

The material fibers normal to the reference line may rotate in the out-of-plane direction by angle  $\gamma(\xi_1)$ , as illustrated in Figure 4. The displacement due to the rotation of any point on the local thickness vector at distance  $\xi_3$  can be approximated as:

$$\delta = \sum_{k=1}^3 \left[ \xi_3 \frac{h}{2} \gamma(\xi_1) \right] N_k(\xi_2) \quad (6)$$

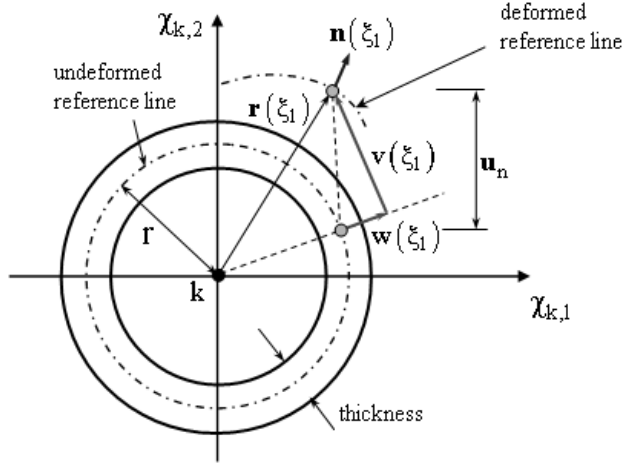


Figure 3: Cross-section deformation

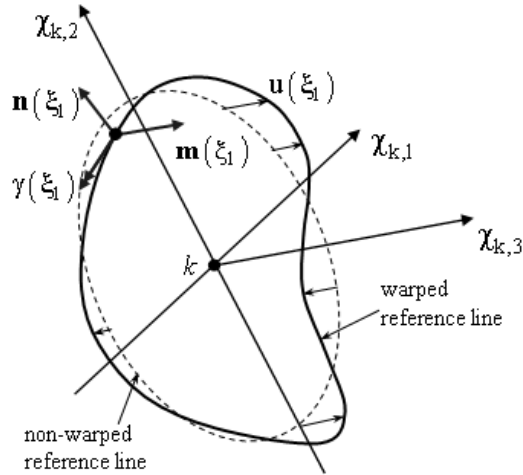


Figure 4: Out-of-plane displacement and rotation of the cross section

Displacement  $\delta$  is directed along the axis  $\mathbf{m}(\xi_1)$ . In case of small displacements the vector  $\mathbf{m}(\xi_1)$  can be taken equal to  $\chi_{k,3}$ . The vector components in the global system are

$$\mathbf{d} = \sum_{k=1}^3 \left[ \xi_3 \frac{h}{2} \gamma(\xi_1) \chi_{k,3} \right] \mathbf{N}_k(\xi_2). \quad (7)$$

The deformation functions  $w(\xi_1)$ ,  $v(\xi_1)$ ,  $\psi(\xi_1)$  and  $\gamma(\xi_1)$  are discretized as follows:

$$w(\xi_1) = a_0 + a_1 \sin \xi_1 + \sum_{n=2,4,6,\dots} a_n \cos n\xi_1 + \sum_{n=3,5,7,\dots} a_n \sin n\xi_1 \quad (8)$$

$$v(\xi_1) = -a_1 \sin \xi_1 + \sum_{n=2,4,6,\dots} b_n \sin n\xi_1 + \sum_{n=3,5,7,\dots} b_n \cos n\xi_1 \quad (9)$$

$$\psi(\xi_1) = \sum_{n=2,4,6,\dots} c_n \cos n\xi_1 + \sum_{n=3,5,7,\dots} c_n \sin n\xi_1 \quad (10)$$

$$\gamma(\xi_1) = \gamma_0 + \gamma_1 \sin \xi_1 + \sum_{n=2,4,6,\dots} \gamma_n \cos n\xi_1 + \sum_{n=3,5,7,\dots} \gamma_n \sin n\xi_1 \quad (11)$$

Coefficients  $a_n$ ,  $b_n$  refer to in-plane cross-sectional deformation (“ovalization” parameters) and  $c_n$ ,  $\gamma_n$  refer to out-of-plane cross-sectional deformation (“warping” parameters). With the geometry and displacement functions given in equations (1), (2), (5) and (7), the position vector of an arbitrary point at the deformed configuration is

$$\mathbf{x} = \sum_{k=1}^3 \left[ \mathbf{x}_k + \mathbf{r}_k(\xi_1) + \xi_3 \frac{h}{2} \mathbf{n}_k(\xi_1) + \xi_3 \frac{h}{2} \gamma(\xi_1) \chi_{k,3} \right] \mathbf{N}_k(\xi_2),$$

where the first two terms within the brackets denote the deformed reference line and the latter two the deformations “through the thickness”.

The stress and strain tensors are described in terms of their components with respect to the curvilinear coordinate system along  $\xi_1$ ,  $\xi_2$  and  $\xi_3$ . The covariant base vectors  $\mathbf{g}_1$ ,  $\mathbf{g}_2$ ,  $\mathbf{g}_3$  are obtained by appropriate differentiation of equation (1) with respect to the coordinates  $\xi_1$ ,  $\xi_2$  and  $\xi_3$ . Note that  $\mathbf{g}_1$  and  $\mathbf{g}_2$  define the shell laminae and  $\mathbf{g}_3$  runs through the thickness. The stress tensor and the incremental strain tensor are written according to

$$\boldsymbol{\sigma} = \sigma^{ij} (\mathbf{g}_i \otimes \mathbf{g}_j)$$

and

$$\Delta \boldsymbol{\varepsilon} = \Delta \varepsilon_{kl} (\mathbf{g}^k \otimes \mathbf{g}^l)$$

where

$$\Delta \varepsilon_{kl} = \frac{1}{2} (\Delta u_{k/l} + \Delta u_{l/k}) \quad \text{and} \quad \Delta u_{k/m} = \frac{\partial (\Delta \mathbf{u})}{\partial \xi_m} \cdot \mathbf{g}_k.$$

Furthermore, shell theory requires that  $\boldsymbol{\sigma} \cdot (\mathbf{m} \otimes \mathbf{m})$  is zero throughout the deformation history, where  $\mathbf{m}$  is the unit normal vector to any lamina. It is readily shown that  $\mathbf{m}$  is equal to  $\mathbf{g}^3 / |\mathbf{g}^3|$ . Similarly, for the tube element it is required that  $\sigma^{33} = \Delta \sigma^{33} = 0$ , whereas the corresponding strain increment component  $\Delta \varepsilon_{33}$  is considered unknown.

For the purposes of the present study, bending is applied about axis  $X_2$  (i.e.  $X_1$ - $X_3$  is the plane of bending). An 5<sup>th</sup> degree expansion ( $n \leq 5$  in equations (8), (9), (10) and (11)) for  $w(\xi_1)$ ,  $v(\xi_1)$ ,  $\psi(\xi_1)$  and  $\gamma(\xi_1)$  is found to be adequate for all cases.

Regarding the number of integration points in the circumferential direction, 19 equally spaced integration points around the half-circumference are used including the two points on the symmetry plane. Five Gauss points are used in the radial (through the thickness) direction. With two Gauss points the tube element is underintegrated with respect to the longitudinal coordinate  $\xi_2$ .

### 3 Gurson material model

In structural steels, after the onset of plastification, progressive material damage can initiate in the form of micro-void nucleation. These voids are first nucleated at second phase particles under the application of external loads, as shown by Brown and Embury [15]. The gradual growth of micro-voids in the material, due to large plastic deformations, will lead to response degradation and eventually fracture.

The initiation and growth of voids within a metallic material can be elegantly simulated by means of the Gurson material model [3]. As compared to other models, the Gurson model has a simpler form and a fewer number of material constants. This pressure dependent plasticity material model contains the classical Von Mises model and is capable of reproducing accurately various aspects of metallic material post-yield response. According to the model, the real material consists of intact material, carrying the stresses, and voids. Numerous alterations and improvements with respect to the yield function and damage evolution, have been suggested by various authors, most notably Tvergaard and Needleman (Tvergaard [4, 5], Chu and Needleman [6], Tvergaard and Needleman [7]), such that it is often referred to as the Gurson-Tvergaard-Needleman (GTN) model. The yield function and plastic potential in the Gurson model are expressed as:

$$F(\sigma) = \frac{q^2}{\bar{\sigma}^2} + \left[ 2q_1 f^* \cosh\left(\frac{3q_2 p}{2\bar{\sigma}}\right) - q_3 f^{*2} \right] - 1, \quad (12)$$

where  $q$  is the effective deviatoric von Mises stress, and  $p$  is the hydrostatic stress. The surface is continuous and hence avoids discontinuity problems. The material dependent parameters  $q_1$ ,  $q_2$  and  $q_3$  are introduced by Tvergaard [4, 5] and affect the shape of the

yield surface. The equivalent tensile flow stress in the matrix material  $\bar{\sigma}$  is a function of the equivalent plastic strain. The parameter  $f^*$  represents the current void volume fraction. The change in void volume fraction during an increment of deformation is partly due to the nucleation of new voids and partly due to the growth of existing ones. As proposed by Chu and Needleman [6] the void nucleation function is assumed to have a normal distribution and is related to the equivalent plastic strain. The void growth rate is proportional to the differential change in the plastic strain of the matrix material.

$$\begin{aligned} df^* &= df^*_{\text{growth}} + df^*_{\text{nucleation}} \\ &= (1-f^*)d\epsilon_{ij}^P \delta_{ij} + A d\bar{\epsilon}^P \end{aligned} \quad (13)$$

$$\text{where } A = \frac{f_N}{s_N \sqrt{2\pi}} \exp \left[ -\frac{1}{2} \left( \frac{\bar{\epsilon}^P - \epsilon_N}{s_N} \right)^2 \right],$$

$\bar{\epsilon}^P$  = the microscopic equivalent plastic strain,

$f_N$  = the volume fraction of void nucleating particles,

$\epsilon_N$  = the mean strain for nucleation and,

$s_N$  = the standard deviation.

### 3.1 Constitutive framework

The strain rate of the matrix material  $\dot{\boldsymbol{\epsilon}}$  can be decomposed in an elastic and a plastic part:

$$\dot{\boldsymbol{\epsilon}} = \dot{\boldsymbol{\epsilon}}^e + \dot{\boldsymbol{\epsilon}}^P \quad (14)$$

In order to take the Bauschinger effect into account kinematic hardening is introduced. The yield function, Eq. (12), becomes:

$$F(\bar{\boldsymbol{\sigma}}) = \frac{\tilde{q}^2}{\bar{\sigma}^2} + \left[ 2q_1 f^* \cosh \left( \frac{3q_2 \tilde{p}}{2\bar{\sigma}} \right) - q_3 f^{*2} \right] - 1, \quad (15)$$

where  $\tilde{q} = q(\bar{\boldsymbol{\sigma}})$  and  $\tilde{p} = p(\bar{\boldsymbol{\sigma}})$ , and

$$\bar{\boldsymbol{\sigma}} = \boldsymbol{\sigma} - \boldsymbol{\alpha}. \quad (16)$$

The center of the yield surface  $\boldsymbol{\alpha}$ , also known as the backstress, is updated as:

$${}^{t+\Delta t} \boldsymbol{\alpha} = {}^t \boldsymbol{\alpha} + d\boldsymbol{\alpha}. \quad (17)$$

Prager [16] assumed that the yield surface moves in the direction of the plastic strain. When hardening parameter  $H_{\text{ISO}}$  is constant the following kinematic hardening rule is linear:

$$d\boldsymbol{\alpha} = \frac{t+\Delta t \bar{\boldsymbol{\sigma}}}{t+\Delta t |\bar{\boldsymbol{\sigma}}|} \cdot H_{\text{KIN}} \cdot d\bar{\boldsymbol{\epsilon}}^{\text{P}} \quad (18)$$

Isotropic hardening is defined as a function of the equivalent plastic strain:

$$\bar{\sigma} = \sigma_0 + H_{\text{ISO}} \cdot \bar{\epsilon}^{\text{P}}, \quad (19)$$

where  $\sigma_0$  represents the initial flow stress in the matrix material. The isotropic hardening response is controlled by parameter  $H_{\text{ISO}}$ .

The associated flow rule is defined as:

$$d\boldsymbol{\epsilon}^{\text{P}} = d\lambda \frac{\partial F}{\partial \boldsymbol{\sigma}} = d\lambda \left( \frac{\partial F}{\partial \bar{p}} \frac{\partial \bar{p}}{\partial \boldsymbol{\sigma}} + \frac{\partial F}{\partial \bar{q}} \frac{\partial \bar{q}}{\partial \boldsymbol{\sigma}} \right) \quad (20)$$

with the standard Kuhn-Tucker conditions:

$$d\lambda \geq 0, \quad F \leq 0, \quad d\lambda \cdot F = 0 \quad (21)$$

The stress tensor can be written as:

$$\bar{\boldsymbol{\sigma}} = -\bar{p}\mathbf{I} + \frac{2}{3}\bar{q}\bar{\mathbf{n}}, \quad (22)$$

where

$$\bar{\mathbf{n}} = \frac{3}{2\bar{q}} \bar{\mathbf{s}}. \quad (23)$$

### 3.2 Numerical implementation

Aravas [1] proposed a numerical algorithm, based on the Euler backward method, for pressure-dependent plasticity models. Integration of Eq. (20) yields:

$$\begin{aligned} {}^{t+\Delta t}\Delta\boldsymbol{\epsilon}^{\text{P}} &= \Delta\lambda \left( \frac{\partial F}{\partial \boldsymbol{\sigma}} \right)_{t+\Delta t} \\ &= \Delta\lambda \left( -\frac{1}{3} \left( \frac{\partial F}{\partial \bar{p}} \right)_{t+\Delta t} \mathbf{I} + \left( \frac{\partial F}{\partial \bar{q}} \right)_{t+\Delta t} {}^{t+\Delta t}\bar{\mathbf{n}} \right) \\ &= \frac{1}{3} \Delta\epsilon_{\text{p}} \mathbf{I} + \Delta\epsilon_{\text{q}} {}^{t+\Delta t}\bar{\mathbf{n}} \end{aligned} \quad (24)$$

where

$$\Delta \varepsilon_p = -\Delta \lambda \left( \frac{\partial F}{\partial \tilde{p}} \right)_{t+\Delta t} \quad \text{and} \quad \Delta \varepsilon_q = \Delta \lambda \left( \frac{\partial F}{\partial \tilde{q}} \right)_{t+\Delta t} \quad (25)$$

Elimination of  $\Delta \lambda$  gives:

$$\Delta \varepsilon_p \left( \frac{\partial F}{\partial \tilde{q}} \right)_{t+\Delta t} + \Delta \varepsilon_q \left( \frac{\partial F}{\partial \tilde{p}} \right)_{t+\Delta t} = 0 \quad (26)$$

First a trial state of stress is obtained, assuming that the entire step is elastic:

$$\boldsymbol{\sigma}^e = {}^t \boldsymbol{\sigma} + \mathbf{D} \cdot \Delta \boldsymbol{\varepsilon}. \quad (27)$$

Isotropic elasticity is assumed so that

$$\mathbf{D}^{ijkl} = \left( K - \frac{2}{3}G \right) g^{ij} g^{kl} + G \left( g^{ik} g^{jl} + g^{il} g^{jk} \right), \quad (28)$$

where  $K$  is the elastic bulk modulus and  $G$  the shear modulus.

For plane stress elements it is required that the stress perpendicular to the surface  $\sigma^{33} = 0$ , whereas the corresponding strain increment component  $\Delta \varepsilon_{33}$  is considered unknown.

If the yield criterion is violated, the final stress at  $t + \Delta t$  is computed through a plastic stress correction, as shown in Figure 5,

$${}^{t+\Delta t} \boldsymbol{\sigma} = {}^t \boldsymbol{\sigma} - \mathbf{D} \cdot \left( \Delta \boldsymbol{\varepsilon} - \Delta \boldsymbol{\varepsilon}^p \right). \quad (29)$$

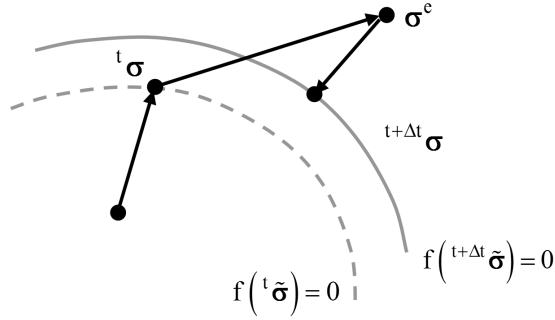


Figure 5: Graphical representation of stress update procedure

Equivalently, the updated stress state at time  $t + \Delta t$  can be written as:

$${}^{t+\Delta t} \tilde{\boldsymbol{\sigma}} = \tilde{\boldsymbol{\sigma}}^e - K \cdot {}^{t+\Delta t} \Delta \varepsilon_p - 2G \cdot {}^{t+\Delta t} \Delta \varepsilon_q \tilde{\mathbf{n}} \quad (30)$$

To enforce the zero stress condition in the radial direction, the strain increment is decomposed in two parts

$$\Delta \underline{\boldsymbol{\varepsilon}} = \Delta \underline{\boldsymbol{\varepsilon}} + \Delta \varepsilon_{33} \boldsymbol{\Psi}_c, \quad (31)$$

and

$$\boldsymbol{\Psi}_c = \mathbf{g}^3 \otimes \mathbf{g}^3 = g^{3k} g^{3m} (\mathbf{g}_k \otimes \mathbf{g}_m).$$

Therefore, equation (30) becomes

$$\begin{aligned} {}^{t+\Delta t} \underline{\boldsymbol{\sigma}} &= \underline{\boldsymbol{\sigma}}^e + \Delta \varepsilon_{33} (\mathbf{D} \boldsymbol{\Psi}_c) - K \Delta \varepsilon_p - 2G \Delta \varepsilon_q \tilde{\mathbf{n}} \\ &= \left( {}^t \underline{\boldsymbol{\sigma}} + \mathbf{D} \Delta \underline{\boldsymbol{\varepsilon}} \right) + \Delta \varepsilon_{33} (\mathbf{D} \boldsymbol{\Psi}_c) - K \Delta \varepsilon_p - 3G \frac{\Delta \varepsilon_q}{\tilde{q}} \tilde{\mathbf{s}} \end{aligned} \quad (32)$$

where

$$\underline{\boldsymbol{\sigma}}^e = {}^t \underline{\boldsymbol{\sigma}} + \mathbf{D} \cdot \Delta \underline{\boldsymbol{\varepsilon}}, \quad (33)$$

and the left superscript  $t + \Delta t$  is omitted for the sake of simplicity in  $p, q$  and  $s$ .

It should be underlined that  $\underline{\boldsymbol{\sigma}}^e$  is not equal to the elastic predictor tensor  $\boldsymbol{\sigma}^e$ . Using equation (22) the hydrostatic and deviatoric parts of the final stress state are now given by the following relationships:

$$\tilde{p} = \underline{p}^e + K \Delta \varepsilon_p - K \Delta \varepsilon_{33} g^{33} \quad (34)$$

$$\tilde{\mathbf{s}} = \underline{\mathbf{s}}^e + 2G \left[ \Delta \varepsilon_{33} \mathbf{y}_c - \frac{3}{2} \frac{\Delta \varepsilon_q}{\tilde{q}} \tilde{\mathbf{s}} \right], \quad (35)$$

where  $\underline{p}^e$  and  $\underline{\mathbf{s}}^{eij}$  are the hydrostatic and deviatoric parts of  $\underline{\boldsymbol{\sigma}}^e$ .

Using equation (35) and the fact the contravariant components of  $\mathbf{y}_c$  are

$$y_c^{km} = g^{3k} g^{3m} - \frac{1}{3} g^{km} g^{33}, \quad (36)$$

it is possible to obtain an expression for the final effective stress  $\tilde{q}$ :

$$\tilde{q} = -3G \Delta \varepsilon_q + \left( \underline{q}^{e2} + 6G \tilde{s}^{e33} \Delta \varepsilon_{33} + 4G^2 \Delta \varepsilon_{33}^2 g^{33} g^{33} \right)^{1/2}, \quad (37)$$

where

$$\underline{q}^e = \sqrt{\frac{3}{2} \mathbf{g}_{ij} \mathbf{g}_{km} \tilde{s}^{eij} \cdot \tilde{s}^{ekm}}}. \quad (38)$$

The condition of zero stress normal to the surface ( $\tilde{\sigma}^{33} = 0$ ) is equivalent to the following condition

$$\tilde{s}^{e33} - \tilde{p} g^{33} = 0 \quad (39)$$

and using equation (35), the following expression is obtained

$$(\tilde{q} + 3G\Delta\epsilon_q)\tilde{p}g^{33} - \left( s^{e33} + \frac{4}{3}G\Delta\epsilon_{33}g^{33}g^{33} \right)\tilde{q} = 0. \quad (40)$$

Equations (26), (15) and (40) constitute a nonlinear algebraic system of  $\Delta\epsilon_p$ ,  $\Delta\epsilon_q$  and  $\Delta\epsilon_{33}$ , which are chosen as the primary unknowns. The equations are solved by means of a Newton-Raphson iteration process at integration point level. During the iterative procedure, the stress is corrected along the hydrostatic and the deviatoric axes  $\tilde{p}$  and  $\tilde{q}$  using equations (34) and (37), respectively.

#### 4 Numerical example

A pipeline bend, as shown in Figure 6, is considered while subjected to a monotonic prescribed rotation  $\kappa_p = 0.2$  rad. The radius of the pipe  $r$  is 198.45 mm. The radius of the bend  $R$  is 609.4 mm. The structure is fixed at node A, so that the end node cannot translate or rotate, whereas the cross-section is free to ovalize, but not to warp. The other end is free to translate perpendicular to the pipe axis but is restrained in the other direction. The cross-section may ovalize, but cannot warp. For the analysis 11 tube elements were used. The numerical results obtained with the tube elements are compared with results obtained with selective integrated Heterosis elements, as introduced by Hughes et al. [17]. For the formulation of the tube element the use of the warping terms is essential. In the elastic domain the results with the tube elements and the shell elements are very close. For the analysis the following material parameters were adopted. The used values for the Gurson parameters are commonly applied for metallic strip material. The initial void volume  $f_0^* = 0.004$  and the initial yield stress is 400 N/mm<sup>2</sup>. The Young's modulus is 205000 N/mm<sup>2</sup> and the Poisson ratio is 0.3. The parameters  $q_1$ ,  $q_2$  and  $q_3$  are 1.5, 1.0 and 2.25 respectively. The hypothetical isotropic hardening parameter  $H_{ISO} = 500$  N/mm<sup>2</sup>. The volume fraction of void nucleating particles  $f_N = 0.04$ , the standard deviation  $s_N = 0.1$  and the mean strain for nucleation  $\epsilon_N = 0.3$ .

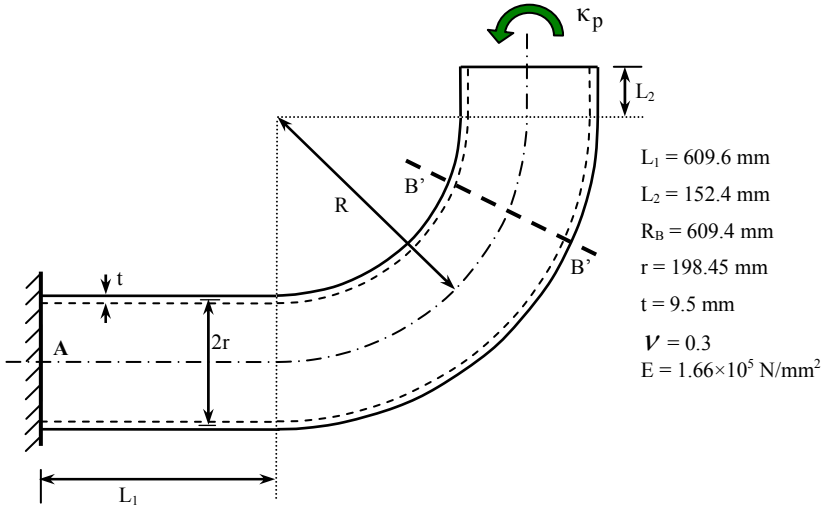


Figure 6: Schematic of pipe structure

Only half the circumference is analyzed due to symmetry. In the following graphs, the stresses and micro-damage  $f^*$  are shown with respect to the hoop direction of the cross section B'-B', where 0 degrees denotes the outside and 180 degrees the inside of the pipe bend.

Figures 7 and 8 show the circumferential stress at the inside of the pipe wall and the longitudinal stress at the outside of the pipe wall, respectively.

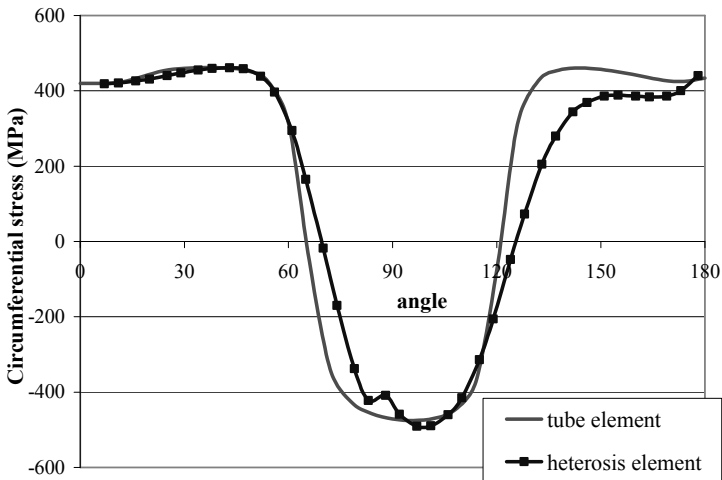


Figure 7: Circumferential stresses at inside of the pipe wall,  $\kappa_p = 0.2 \text{ rad}$

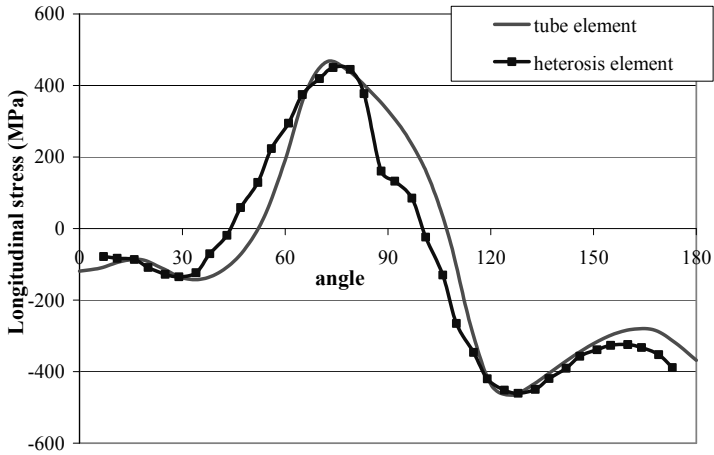


Figure 8: Longitudinal stresses at outside of the pipe wall,  $\kappa_p = 0.2 \text{ rad}$

The onset of plasticity is at the inside of the tube due to the circumferential stress, as shown in Figure 9a. Due to the longitudinal stress at the outside of the pipe wall, micro damage will also grow at the inside of the pipe bend as shown in Figure 9b. The red colour corresponds to the initial void volume  $f_0^*$  and the blue colour to the maximum value.

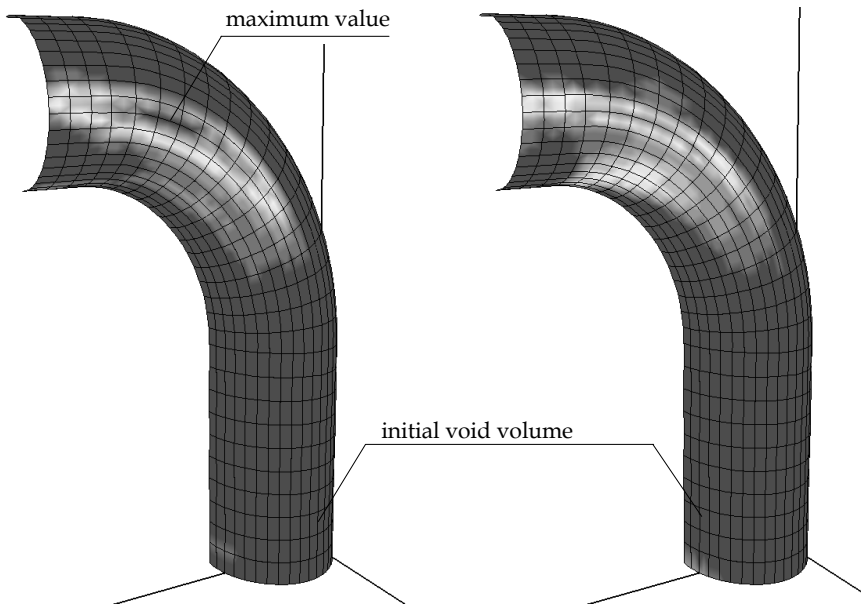


Figure 9: Damage development at inside of pipe wall and at outside of pipe wall (Heterosis elements)

In Figure 10 the development of micro-damage  $f^*$  at the inside of the pipe wall is shown. When the tube elements are used, the maximum developed damage is less than the damage with the Heterosis shell element, but the zone is wider. Analysis of the pipe structure with different integration schemes or number of elements do not show a significant difference, as the plastic strains are not large. The observed difference in damage development is due to the algorithms which are used to describe the deformation of the elements.

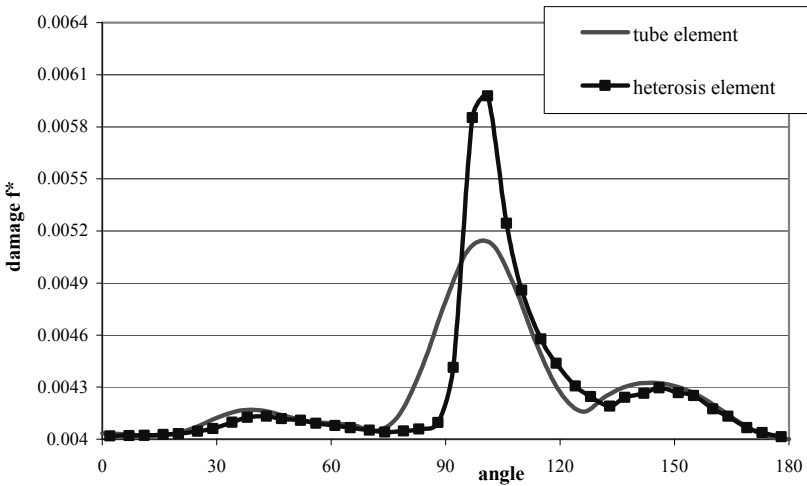


Figure 10: Damage development at inside of the pipe wall,  $\kappa_p = 0.2 \text{ rad}$

## 5 Conclusions

In this paper the stresses and micro-damage development in steel pipelines are analyzed by means of finite tube elements in combination with the Gurson constitutive model. The results are compared with the stresses and damage development determined with finite shell elements in combination with the same material model. The stresses in longitudinal and circumferential direction in the pipeline determined with both elements show a very good agreement. The maximum damage development with the tube elements is lower than with the shell elements, but the predicted shape and area under the curve are close.

## References

- [1] Aravas, N. (1987) 'On the numerical integration of a class of pressure-dependent plasticity models' in *Int. J. Num. Meth. Eng.*, Vol. 24, pp. 1395-1416.
- [2] Brush, D.O., Almroth, B.O. (1975) *Buckling of Bars, Plates, and Shells*, McGraw-Hill.
- [3] Gurson, A.L. (1975) *Plastic flow and fracture behavior of ductile materials incorporating void nucleation, growth, and interaction*. Ph.D. thesis.
- [4] Tvergaard, V. (1981) 'Influence of Voids on Shear Band Instabilities under Plane Strain Conditions' in *Int. J. Fract.*, Vol. 17, pp. 389 - 407.
- [5] Tvergaard, V. (1982) 'On localization in Ductile Materials Containing Spherical Voids' in *Int. J. Fract.*, Vol. 18, pp. 237 - 252.
- [6] Chu, C.C., Needleman, A. (1980) 'Void Nucleation Effects in Biaxially stretched sheets' in *Journal of Engineering Materials Technology*, Vol. 102, pp. 249 - 256.
- [7] Needleman, A., Tvergaard, V. (1991) 'An analysis of Dynamic Ductile Crack Growth in a Double Edge Cracked Specimen' in *Int. J. Fract.*, Vol. 49, pp. 41 - 67.
- [8] Karamanos, S.A., Tassoulas, J.L., (1996) 'Tubular Members. I: Stability and Preliminary Results' in *Journal of Engineering Mechanics ASCE*, Vol. 122, pp. 64 - 71.
- [9] Karman, Th. von (1911) 'Ueber die Formänderung dünnwandiger Rohre' in *Zeitschrift des Vereines deutscher Ingenieure*, Vol. 55, pp. 1889 - 1895.
- [10] Vigness, I. (1994) 'Elastic properties of Curved Tubes' in *Transactions of the ASME*, Vol. 65, pp. 105 - 120.
- [11] Clark, R.A., Reissner, E. (1951) 'Bending of curved tubes' in *Advances in Applied Mechanics* Vol. 2, pp. 93 - 122.
- [12] Rodabaugh, E.C., George, H.H. (1957) 'Effect of Internal Pressure on Flexibility and Stress Intensification Factors of Curved Pipe or Welding Elbows' in *Trans. ASME*.
- [13] Bathe, K.J., Almeida, C.A. (1980) 'A Simple and Effective Pipe Elbow Element - Linear Analysis' in *ASME Journal of Applied Mechanics*, Vol. 47, pp.93 - 100.
- [14] Bathe, K.J., Almeida, C.A. (1982) 'A Simple and Effective Pipe Elbow Element - Interaction Effects' in *ASME Journal of Applied Mechanics*, Vol. 49, pp. 165 - 171.
- [15] Brown, L.M., Embury, J.D. (1973) 'The initiation and growth of voids at second-phase particles' in *Proceedings of the Third International Conference on Microstructure and Design of Alloys*, pp. 164 - 169. Institute of Metals and Iron and Steel, London.
- [16] Prager, W. (1956) 'A New Method of Analyzing Stress and Strains in Work-Hardening Plastic Solids' in *Journal of Applied Mechanics*, Vol. 23, pp. 493 - 496.

- [17] Hughes, T.J.R., Cohen, M. (1978) 'The 'Heterosis' Finite Element for Plate Bending' in *Computers and Structures*, Vol. 9, pp. 445 - 450.